Al–Cu intermetallic coatings processed by sequential metalorganic chemical vapour deposition and post-deposition annealing

Lyacine Aloui, Thomas Duguet, Fanta Haidara, Marie-Christine Record, Diane Samélor, François Senocq, Dominique Mangelinck, Constantin Vahlas

HAL Id: hal-01756334

https://amu.hal.science/hal-01756334

Submitted on 17 Jan 2022

Al–Cu intermetallic coatings processed by sequential metalorganic chemical vapour deposition and post-deposition annealing

Lyacine Aloui [a], Thomas Duguet [a,*], Fanta Haidara [b], Marie-Christine Record [b], Diane Samélor [a], François Senocq [a], Dominique Mangelinck [b], Constantin Vahlas [a]

[a] CIRIMAT, Université de Toulouse - CNRS, 4 allée Emile Monso, BP-44362, 31432 Toulouse Cedex 4, France
[b] IM2NP, Université Paul Cézanne - CNRS, Faculté de St Jérôme, Case 142, 13397 Marseille Cedex 20, France

ABSTRACT

Sequential processing of aluminum and copper followed by reactive diffusion annealing is used as a paradigm for the metalorganic chemical vapour deposition (MOCVD) of coatings containing intermetallic alloys. Dimethylethylamine alane and copper N,N′-di-isopropylacetamidinate are used as aluminum and copper precursors, respectively. Deposition is performed on steel and silica substrates at 1.33 kPa and 493–513 K. Different overall compositions in the entire range of the Al–Cu phase diagram are obtained by varying the relative thickness of the two elemental layers while maintaining the overall thickness of the coating close to 1 μm. As-deposited films present a rough morphology attributed to the difficulty of copper to nucleate on aluminum. Post-deposition annealing is monitored by in situ X-ray diffraction, and allows smoothening the microstructure and identifying conditions leading to several Al–Cu phases. Our results establish a proof of principle following which MOCVD of metallic alloys is feasible, and are expected to extend the materials pool for numerous applications, with innovative thin film processing on, and surface properties of complex in shape parts.

1. Introduction

Al–Cu intermetallic compounds present attractive properties in applications such as interconnects for integrated circuits [1] or corrosion resistant coatings [2]. Al–Al$_2$Cu composites feature enhanced Young's modulus, good compressive strength and reasonably good compressive ductility [3]. In addition, Al and Cu are reasonably inexpensive, and easily available.

Processing of Al–Cu and, more generally of intermetallic alloy coatings by metalorganic chemical vapour deposition (MOCVD) is expected to extend their implementation in surface engineering. Especially, thanks to the possibility to operate in surface reaction controlled regime, MOCVD allows surface treatment of complex-in-shape items such as glass moulds, turbine blades and vanes in aeronautic industries, or porous preforms whose internal surface may be functionalized for the preparation of supported catalysts. Versatility, cost effectiveness, environmental compatibility, and the possibility to process films containing thermodynamically metastable phases, are additional advantages of MOCVD processes. Finally, the use of molecular precursors allows operating at low to moderate temperatures, thus extending the targeted applications spectrum so as to cover temperature-sensitive substrates.

The price to pay for this high potential is the need to tackle the challenges imposed by the complex gas phase and surface chemistries. In addition to mastering the deposition reaction, these challenges also concern the design of the precursors upstream the MOCVD process, the engineering of the MOCVD apparatus in terms of precursor vapour generation, energy delivery means, and dynamical in situ and on line diagnostics to monitor gas and surface reactions. The inherent difficulty for the establishment of a robust MOCVD process is further amplified in the case of coatings containing several elements and potentially intermetallic phases, mainly because of the limited width of their stability domains, and the far-from-equilibrium initial state which can lead to unpredicted transitions [4]. Moreover, such a process for the preparation of multimetallic coatings must involve the use of compatible precursors for the deposited elements. The general criteria qualifying an inorganic or molecular compound as precursor for CVD processes were discussed by Maury et al. [5,6]. In the case of the MOCVD of intermetallic compounds there are additional ones such as (a) similar transport behaviours, (b) absence of heteroatoms in the ligands which may react with the other metal, (c) compatible decomposition schemes, and if possible (d) belonging to a common family of compounds. Until now, this situation resulted in limited investigation of MOCVD for the co-deposition of intermetallic alloy films.

Reports on the MOCVD of Al–Cu were published in the nineties involving aluminum alane and copper phosphine precursors [7,8]. However, they concern films with low copper concentration, at the level of 1 wt.%, targeting the doping of Al-based interconnections in microelectronics rather than the processing of coatings containing intermetallic phases.

The above mentioned constraints can be partially circumvented if the preparation of the coating proceeds in two steps. Namely, sequential deposition of the elements in the form of bi- or multi-layers, is followed by an appropriately tuned annealing which leads to the formation of the targeted phases. This latter solution, applied in the processing of Al/Cu bilayers, is adopted in the present study. Optimization of the deposition reactor, processing of the Al and Cu unary films, investigation of their decomposition mechanisms, and kinetic modelling of the MOCVD process are presented elsewhere ([9,10] and references therein).

The article is presented as follows. The experimental protocol involving MOCVD of Al and Cu, and post-deposition annealing is presented in details, first. Then, the microstructure and composition profiles of the as-processed Al-rich and Cu-rich bilayers are compared. Finally, microstructure and phase transitions of the annealed coatings are presented and discussed, prior to providing concluding remarks.

2. Material and methods

Depositions are performed in the experimental setup described in details and modeled in Ref. [11]. The setup is composed of a stagnant flow, cylindrical, stainless steel reactor. The deposition chamber features a double envelope allowing the monitoring of walls temperature through the circulation of thermally regulated silicon oil. A turbomolecular pump ensures a base pressure of 1.3×10^{-4} Pa. The pumping group is protected from the corrosive by-products by a liquid nitrogen trap. Gas is distributed through a showerhead system, described and modeled in Ref. [12]. Gases are fed through electropolished stainless steel gas lines with VCR fittings and their flow rate is controlled by computer driven mass flow controllers.

5 mm × 10 mm up to 20 mm × 20 mm 304L stainless steel coupons are used as representative of technologically interesting substrates. Thermally oxidized silicon (140 nm SiO_2) coupons are used for the ease of cross sections preparation for observation by scanning electron microscopy (SEM), and for X-ray diffraction analyses (XRD). Substrates are placed horizontally on a 58 mm diameter susceptor standing below the showerhead. They are heated by a resistance coil gyred just below the surface of the susceptor. Stainless steel substrates are polished down to 4000 SiC paper grade and are sonicated in acetone and anhydrous ethanol. Silicon wafers are degreased in a 70% H_2SO_4–30% H_2O_2 solution, rinsed with deionized water and dried under argon stream before use. A set of five stainless steel and five SiO_2 substrates is used in each run. Substrates are exposed to atmosphere for a limited time during their transfer between the preparation lab and their loading into vacuum. Prior to deposition, in situ radio frequency (RF) Ar–10% H_2 plasma etching is applied with input power 40 W at 120 kHz, in conditions 160 Pa and 493 K, for 30 min with the aim to recover an organic-pollution-free steel or silica surface. In all experiments the operating pressure and the temperature of the reactor walls are fixed at 1.33 kPa and 368 K, respectively.

Adduct grade DMEAA (SAFC Hitech) is used as-received in a stainless steel bubbler. It is maintained at 281 K by immersion in a thermoregulated water bath. The corresponding saturated vapour pressure is 99 Pa. The DMEAA bubbler is maintained at this temperature during the entire period of its service in order to avoid degradation of the precursor [13]. 25 standard cubic centimetres (sccm) of 99.9992% pure nitrogen (Air Products) bubbles through the Al precursor. Assuming saturation of the gas phase, these conditions lead to an upper limit of the DMEAA flow rate equal to 2 sccm [14]. The total flow rate is completed to 327 sccm by adding 300 sccm of N_2 as a dilution gas. Deposition temperature is fixed at 493 K. It has been previously shown that in these conditions a mean nucleation delay of 7 min precedes initiation of the growth of Al. Nucleation delay is determined by observation of change of the colour of the surface and is the same for SiO_2 and stainless steel samples. Al growth rate is measured at certain positions over the susceptor, through the weight gain of each sample [10]. Weight gain is preferred to thickness measurement since film porosity and roughness induce an overestimation of the growth rate. For instance, SEM analysis of the cross-section of an Al (resp. Cu) sample showed a 1300 nm (resp. 110 nm) thick film, whereas the thickness determined by weight measurement was 400 nm (resp. 45 nm), only. Al growth rate is mapped as being constant at 12.6 μmol cm^{-2} h^{-1} on the central part of the susceptor and gradually increasing beyond a radius of 15 mm to reach 15.6 μmol cm^{-2} h^{-1} at the edge of the susceptor, averaging 13.3 μmol cm^{-2} h^{-1} on the entire heated surface.

[Cu(i-Pr-Me-AMD)]$_2$ (NanoMePS, www.nanomeps.fr, last accessed October 7, 2011) is used as-received for Cu deposition. This precursor is appropriate for use in a process involving CVD of Al from DMEAA because (a) the two processing conditions windows partially overlap, (b) it contains neither oxygen nor halogens in the ligands, nor it requires oxygen containing co-reactants for the deposition of copper [9]. [Cu(i-Pr-Me-AMD)]$_2$ is manipulated in glove box and is conditioned in a packed bed loaded in a homemade sublimator composed of a full stainless steel body, a frit and VCR fittings. A load of 500 mg of fresh compound is used in each run. During deposition the precursor is maintained at 368 K with thermally regulated heating tapes, this temperature corresponding to a saturated vapour pressure of 36 Pa [9]. 50 sccm of N_2 are fed through the copper precursor corresponding to an upper limit of the flow rate of [Cu(i-Pr-Me-AMD)]$_2$ equal to 1.2 sccm. 50 sccm of 95% pure hydrogen (Air Products) is used as reducing gas. The relatively low purity of H_2 does not impact the purity of the deposited Cu. Similar to the deposition of Al, the total flow rate is completed to 326 sccm by adding 225 sccm of N_2 dilution gas. Cu deposition is performed at 513 K. The mean growth rate of Cu in these conditions was previously determined by weight gain to be equal to 0.3 μmol cm^{-2} h^{-1} [15].

The deposition protocol consists in (a) establishing flow rates in all the gas lines, bypassing the precursor vessels, (b) establishing the targeted temperature at each part of the setup except for the copper sublimator, (c) performing the deposition of Al, (d) bypassing the DMEAA bubbler for 30 min, (e) heating the copper sublimator to 368 K (10 min) and increasing the temperature of the susceptor to 513 K, (f) performing deposition of Cu, and (g) bypassing the precursor vessels while cooling down the susceptor. This protocol presents the drawback of maintaining the free surface of the deposited Al during 40 min (steps (d) and (e)) prior the deposition of Cu, running the risk of contamination of the Al/Cu interface by residual oxygen. However, contamination level is lower than the one obtained if using O-containing Cu precursors.

Several deposition runs are performed in the same conditions, the difference being the durations of the deposition of Al (between 20 min and 57 min) and Cu (between 170 min and 960 min).

Post-deposition annealing is applied to the as-processed Al/Cu bilayers in order to investigate reactive diffusion, and obtain coatings containing different intermetallic Al–Cu phases. In situ XRD measurements in Bragg–Brentano configuration are performed during heat treatments in two instruments, operating with Cu Kα, Ni filtered radiation: a Bruker D8 Advance, fitted with a Vantec Super Speed detector and a Philips X'pert. They are equipped with
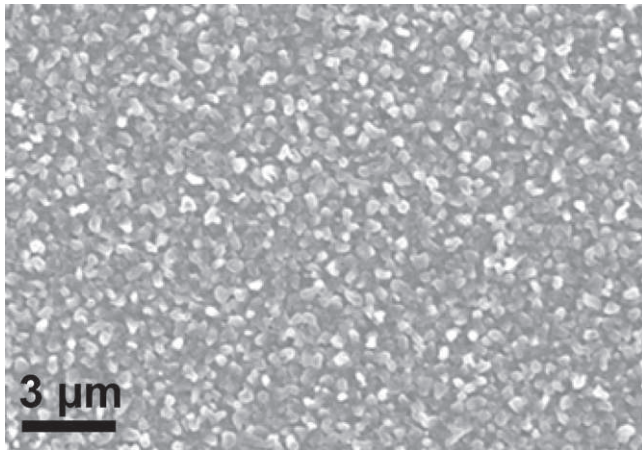
Fig. 1. Surface SEM micrograph of an Al film deposited on thermally grown silica in the adopted conditions with in situ plasma pre-treatment.

a MRI (under vacuum) and an Anton Paar HTTK (under controlled atmosphere) high temperature chambers, respectively. The X-ray diffractograms are recorded from room temperature up to 928 K by steps of 30°. Crystallographic characteristics of the as-deposited and annealed coatings are determined by XRD in grazing incidence using a Seifert XRD 3000TT instrument (Cu Kα, graphite diffracted beam monochromator).

The arithmetic average roughness (R_a) of as-deposited bilayers and post annealed coatings is determined with a Zygo MetroPro, New View 100 optical profilometer. Their morphology is evaluated with a LEO 435-VP scanning electron microscope. The elemental composition of the coatings is determined by Electron Probe Micro-Analysis (EPMA) with a CAMECA SX-50 apparatus, equipped with three wavelength dispersive spectrometers. Depth profiles are determined by radio frequency glow discharge optical emission spectrometry (RF GD-OES) with a Horiba Scientific GD-Profiler2. RF GD-OES uses a low pressure plasma for fast sputtering (few μm/min) of the surface of the sample and excitation of the sputtered atoms. Light emitted by sputtered atoms during species de-excitation is collected by a polychromator that is able to detect all elements far from UV to low infrared (including H, O, C or N species). The use of radio frequency suppresses the constraint of using conducting samples, hence oxidized Si substrates can be characterized readily.

3. Results and discussion

3.1. As-deposited films

As-deposited films are systematically composed of elemental Al and Cu. According to depth profiling results, reactive diffusion at the Al–Cu interface is initiated during the deposition of Cu (deposition at 513 K), but the quantity of intermetallic phases is not enough to reveal corresponding peaks in the X-ray diffractograms. The content of heteroatoms due to the precursor ligands or to the residual atmosphere of the reactor vessel (oxygen, nitrogen, carbon) is systematically below the detection limit of EPMA (<1 at.%), with our apparatus.

Fig. 1 presents a SEM micrograph of Al deposited on thermally grown silica after in situ plasma pre-treatment of the substrate (Fig. 1a) plasma pre-treatment yielding a smoother surface. R_a value for this film is 0.024 μm, to be compared with 0.105 μm for unprocessed substrates.

Cu deposition on Al films provides bilayers whose surface characteristics depend on the quantity per unit surface of the deposited Cu. Small quantities of deposited Cu, corresponding to a high Al:Cu
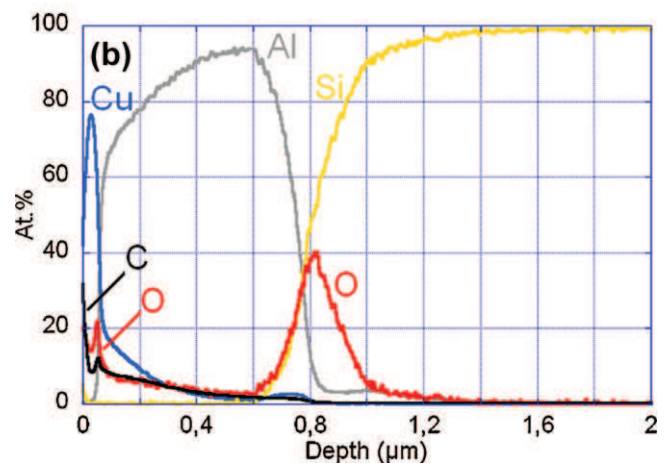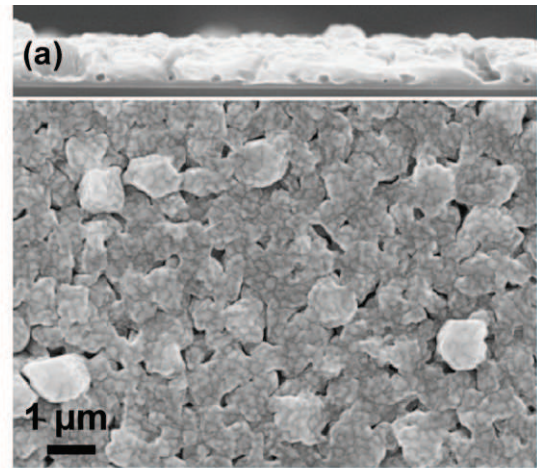

Fig. 2. Al-rich Al/Cu bilayer with overall composition 11 at.% Cu. (a) Surface (bottom) and cross section (top) SEM micrographs and (b) RF GD-OES depth profile of a bilayer formed on silica.

ratio, do not markedly modify the morphology of the film with regard to the one shown in Fig. 1. A SEM cross section and a surface view of an as-deposited bilayer with an overall composition of 11 at.% Cu is shown in Fig. 2a. The cross section of the film is typical of that of CVD Al [16]. R_a of the film equals 0.087 μm and the surface microstructure is organized in two levels: an Al layer of approx. 1 μm, and a thinner Cu layer of 0.1 μm.

A better insight in the organization of the bilayer is obtained by performing the RF GD-OES depth profile analysis. Fig. 2b shows the sample elemental composition vs. depth. Four layers can be identified. Starting from the surface, we determine that the Cu layer is 0.08 μm-thick, and that it contains C and O. Cu sits on top of a 0.75 μm-thick Al layer that also contains C and O contaminants. It is interesting to note that Cu diffuses deep below the surface (approx. down to 0.8 μm). A small Cu peak between 0.65 and 0.80 μm depth may correspond to fast diffusion of Cu in preferential diffusion paths and Cu silicides formation, or to the abrupt change of the sputtering rate at the Al/silica interface.

C and O peaks present at the Al/Cu interface may correspond to a slight oxidation of the Al surface before Cu deposition starts. The third layer (between 0.8 and 1.0 μm depth) corresponds to the thermally oxidized SiO_x layer, followed by the pure Si wafer (depth >1.4 μm).

Topography of our samples has to be considered for RF GD-OES analyses because sputtering occurs on a large surface area (2 mm diameter anode) [17]. First, samples present a rough morphology with more or less dense regions, porosities, and such. This
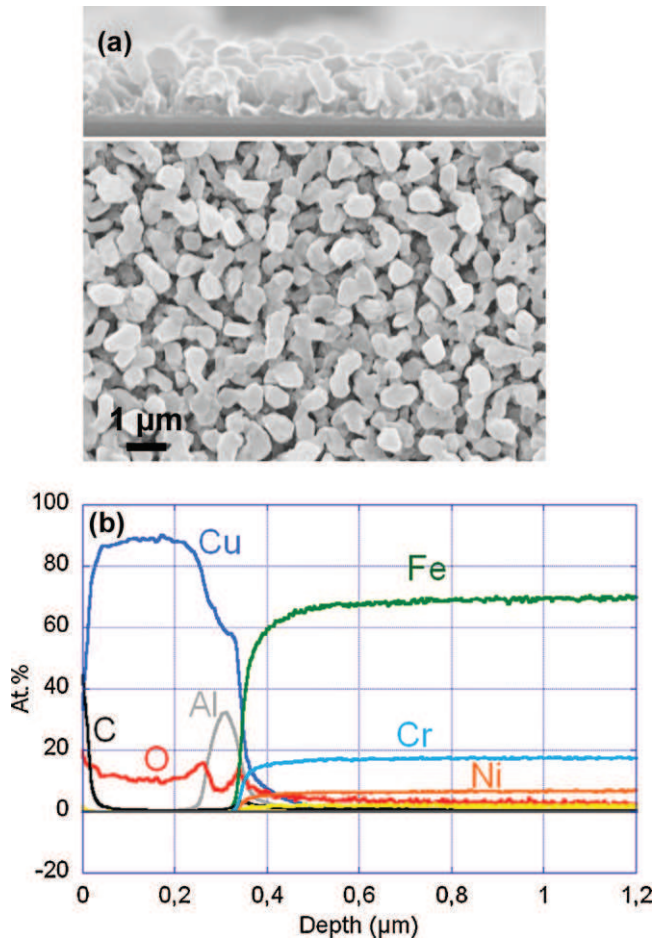
Fig. 3. Cu-rich Al/Cu bilayer with overall composition 90 at.% Cu. (a) Surface (bottom) and cross section (top) SEM micrographs of an as-processed sample grown on silica. (b) GD-OES depth profile of a bilayer formed on stainless steel.

can result in the simultaneous sputtering of the surface and of a deeper feature, such as an open porosity. Therefore, it is important to carefully evaluate contaminants level and sharp interfaces composition. With flat, dense, and smooth samples, a flat-bottom crater is created with RF GD-OES that corresponds to a pseudo-layer-by-layer etching. With imperfect samples we suspect that a deeper (next) layer may be sputtered before the end of the previous layer sputtering. In the profile plot, this would correspond to visualizing two (or more) elements coming from different layers at the same time even whereas the chemical interface is actually sharp, normal to the surface. Another point is the absence of ultra-high vacuum that might imply that O, H, and C compositions are largely overestimated compared to real values in the films. EPMA measurements after Al and Cu depositions show contaminants levels under the apparatus detection limit (<1 at.%). Additionally, hydrogen is known to have a substantial effect on the intensities of the optical emission spectra [18]. We ignored this effect, and do not present hydrogen in the quantitative profiles, although H signal was acquired. Since the signals are normalized to 100%, neglecting hydrogen induces another uncertainty on the overall composition.

Large quantities of deposited Cu, corresponding to Al–Cu coatings with high Cu content yield as-deposited bilayers with rough surface. Elemental composition of the following samples is 90–92 at.% Cu, depending on their relative position in the MOCVD reactor. Fig. 3a presents a cross section and surface SEM micrographs of an as-processed film on thermally grown silica. The cross section reveals a porous microstructure which was developed on a thin sublayer of Al. This is also illustrated on the surface view

of the sample which presents a microstructure with R_a equal to 0.161 μm, typical to that of CVD Cu [15]. Density functional theory (DFT) calculations revealed that the first stage of nucleation of Cu on atomically smooth surface of Al is not energetically favoured. Adsorbed Cu adatoms are thus expected either to segregate beneath the surface of Al or to form nucleus on sites of high energy, such as other surface adatoms or defects [19]. When nucleation of Cu is achieved, additional Cu adatoms are expected to diffuse on the surface so as to contribute to the growth of the existing Cu grains. Although not taking into account the proper reaction scheme of the MOCVD process and the initial surface state, this growth mode is at least partially responsible for the final rough microstructure of the film; i.e. through the formation of a discontinuous film with important open porosity.

The GD-OES elemental profile of an Al/Cu bilayer formed on stainless steel is shown in Fig. 3b. We identify different layers from this plot. The extreme surface layer (approx. 20 nm) corresponds to adsorbed C and O species. Then, a Cu layer extends over 0.25 μm. It seems to contain 10 at.% O. Considering the comments made above and because EPMA does not detect O, we assume that the effective O content is lower. This layer is followed by a slightly oxidized Al/Cu interface, as shown by the O peak at 0.25 μm. The following 0.1 μm-thick Al layer shows a very high content of Cu that confirms the fast diffusion of Cu at deposition temperature (513 K). We do not know where/how diffusion occurs, though. The fact that X-ray diffraction results show fcc-Al at low temperatures implies that at most an (Al) solid solution is formed, but obviously not with 59 at.% Cu as it seems to be at 0.3 μm depth. Again, excited Cu* and Al* atoms co-exist in the GD plasma because they are sputtered at the same time, but not necessarily because they co-exist in the Al layer. Finally, the interface with stainless steel is complex, with possible interdiffusion of Al and Cu into the substrate and of Fe and alloying elements into the coating.

3.2. Post-deposition annealing

Fig. 4 presents two high temperature X-ray diffractograms obtained for coatings containing 19 at.% Cu (a) and 35 at.% Cu (b). The thickness of both samples is approx. 1 μm after annealing, as determined by SEM cross section analyses. Their microstructure is compact and homogeneous (no layers are distinguishable) showing that the whole coating thickness is alloyed. XRD intensity levels are represented by the gray scale. In both samples, reaction between Al and Cu during heat treatment results in the evolution of the Al and Cu peaks, and the appearance of peaks corresponding to intermetallic compounds. Peaks of Al and Cu either disappear or are shifted (Fig. 4a). After heat treatment, sample (a) is composed of a mixture of solid solution α-(Al), θ-Al$_2$Cu, and a small amount of Cu for which a peak is still visible. Sample (b) is single-phased, with only η-AlCu peaks. Heat treatment of sample (a) was stopped at 853 K because of the vanishing of the diffraction peaks at this temperature. This is attributed to the appearance of a liquid phase as can be concluded by the eutectic reaction of the Al–Cu phase diagram occurring at 821 K for alloys with compositions between (Al) and Al$_2$Cu [20]. The same conclusion is drawn for sample (b) where annealing should have resulted in the formation of a two-phase sample composed of θ-Al$_2$Cu and of 12% weight fraction of η-AlCu. The vanishing of the Al$_2$Cu peaks above 823 K (550°C in Fig. 4b) may correspond to the melting of Al$_2$Cu, that should occur above 863 K.

According to the in situ X-ray analysis, Al and Cu first react to form Al$_2$Cu. If the composition is rich enough in Cu (sample b), then Al$_2$Cu reacts with the remaining Cu to form AlCu, above 823 K. For sample (b), we suspect that γ-Al$_4$Cu$_9$ is also formed along with θ-Al$_2$Cu. Its main diffraction peak (3 3 0) appears at about the same position as Al(2 0 0) which renders its identification ambiguous.
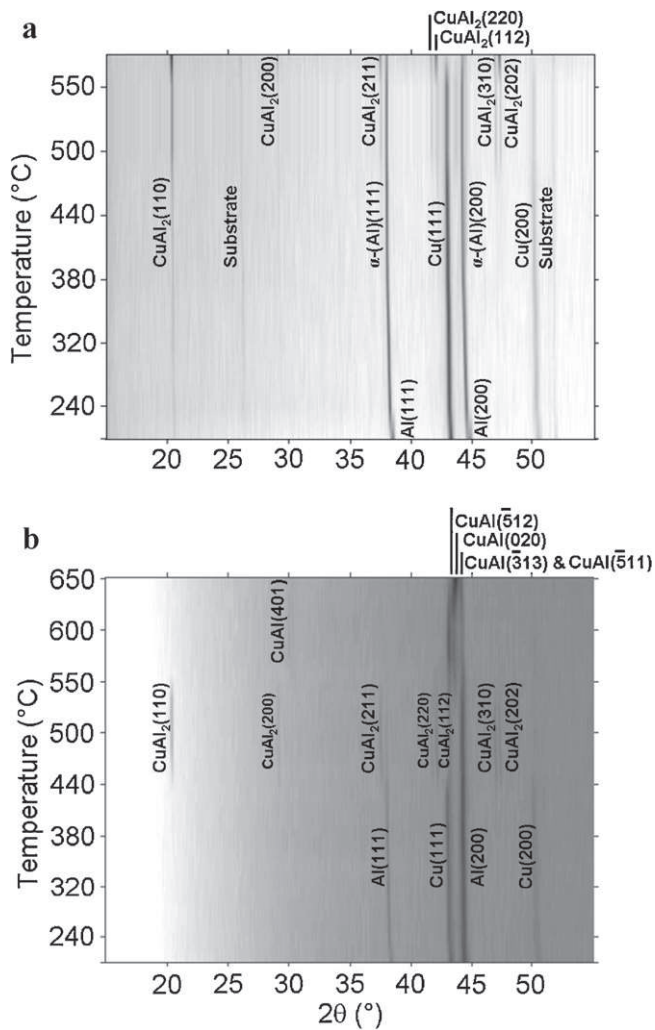
Fig. 4. X-ray diffractograms recorded as a function of temperature during post-deposition annealing for samples with composition 19 at.% Cu (a) and 35 at.% Cu (b).

However if Al_4Cu_9 is formed, it is characteristic of a transient phase because it would appear and disappear during the formation of Al_2Cu while both Al and Cu are still present [21].

Fig. 5 presents a surface SEM view of the sample containing 19 at.% Cu after annealing at 853 K. The surface appears as being
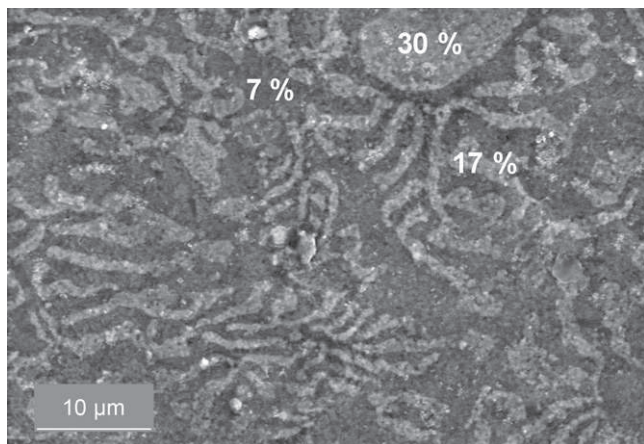

Fig. 5. Low magnification SEM surface view of a film with overall composition 19 at.% Cu. Notations correspond to atomic percent of Cu.

non-homogeneous with at least two zones, illustrated by curved bright stripes and a grey background. The value of R_a in this case is $0.212\,\mu m$. EPMA analysis revealed the presence of three zones with variable elemental composition, namely 5–8, 17 and 30 at.% Cu. Although the probe size of the instrument is $5\,\mu m$; i.e. larger than the typical length scale of the observed features, these results confirm the heterogeneity of the sample. This microstructure is due to the thermal history of the film which was cooled down from a partially liquid state to room temperature. The composition of the three zones of the film fits the eutectic equilibrium at the Al-rich side of the Al–Cu phase diagram, involving 3 at.% Cu solid solution fcc α-(Al), θ-Al_2Cu and a liquid phase at 17 at.% Cu. The presence in the film of a phase whose composition corresponds to the liquid phase is attributed to the relatively high cooling rate of $30°$/min. Based on these remarks, elemental compositions were noted in the three phases of the micrograph in Fig. 5. The ultimate microstructure of such coatings is compact. It confirms the determined overall composition of the coating, and illustrates the coherence between the overall composition of the coating and the corresponding phase equilibrium, at least in this region of the phase diagram.

4. Conclusions

Bilayers of Cu and Al were deposited by MOCVD at 1.33 kPa and temperatures 493 K and 513 K on stainless steel and oxidized Si substrates with the aim to process Al–Cu intermetallic alloy films. Dimethylethylamine alane and copper N,N′-di-isopropylacetamidinate provided pure Al and Cu films, respectively. Al films are smooth, whereas subsequently deposited Cu yields surfaces whose roughness increases with increasing thickness. Reactive diffusion is observed through post-deposition annealing, inducing the formation of Al–Cu intermetallic phases. In situ X-ray diffraction measurements during heat treatment allow investigation of the reaction path. Deposition of different relative thicknesses of Cu and Al films lead to different sample compositions, and allows the exploration of different phase spaces of the Al–Cu phase diagram. Films containing θ-Al_2Cu, η-AlCu, and likely γ-Al_4Cu_9 are obtained.

Forthcoming publications will focus on the investigation of the samples with an intermediate Cu content, and of appropriate annealing conditions, with the aim of creating single-phase intermetallic coatings of technological interest (γ-Al_4Cu_9 or ζ-Al_3Cu_4, for instance).

The obtained results show that MOCVD associated with post-deposition heat treatment is a valid way to obtain films of intermetallic alloys, paving the way to conformal deposition of this type of materials for numerous application fields.

References

[1] P.-P. Choi, T. Al-Kassab, R. Kirchheim, Scripta Mater. 53 (2005) 323–327.
[2] W.R. Osorio, J.E. Spinelli, C.M.A. Freire, M.B. Cardona, A. Garcia, J. Alloys Compd. 443 (2007) 87–93.
[3] C.J. Hsu, P.W. Kao, N.J. Ho, Scripta Mater. 53 (2005) 341–345.
[4] C. Vahlas, Chemical vapor deposition of metals: from unary systems to complex metallic alloys, in: E. Belin-Ferré (Ed.), Complex Metallic Alloys: Surfaces and Coatings, World Scientific, Singapore, 2010, pp. 49–81.

[5] F. Maury, J. de Physique IV C5 (1995) 449–463.

[6] F. Maury, L. Gueroudji, C. Vahlas, Surf. Coat. Technol. 86–87 (1996) 316–324.

[7] T. Katagiri, E. Kondoh, N. Takeyasu, T. Nakano, H. Yamamoto, T. Otha, Jpn. J. Appl. Phys., Part 2 32 (1993) L1078–L1080.

[8] E. Kondoh, Y. Kawano, N. Takeyasu, T. Ohta, J. Electrochem. Soc. 141 (1994) 3494–3499.

[9] V.V. Krisyuk, L. Aloui, N. Prud'homme, S. Sysoev, F. Senocq, D. Samélor, C. Vahlas, Electrochem. Solid-State Lett. 14 (2011) D26–D29.

[10] T.C. Xenidou, N. Prud'homme, C. Vahlas, N.C. Markatos, A.G. Boudouvis, J. Electrochem. Soc. 157 (2010) D633–D641.

[11] T.C. Xenidou, A.G. Boudouvis, N.C. Markatos, D. Samélor, F. Senocq, A.N. Gleizes, N. Prud'homme, C. Vahlas, Surf. Coat. Technol. 201 (2007) 8868–8872.

[12] T.C. Xenidou, A.G. Boudouvis, N.C. Markatos, N. Prud'homme, L. Aloui, C. Vahlas, ECS Trans. 25 (2009) 1053–1060.

[13] H. Matsuhashi, C.-H. Lee, T. Nishimura, K. Masu, K. Tsubouchi, Mater. Sci. Semicond. Process. 2 (1999) 303–308.

[14] C. Vahlas, B. Caussat, F. Senocq, W.L. Gladfelter, L. Aloui, T. Moersch, Chem. Vap. Deposition 13 (2007) 123–129.

[15] V.V. Krisuyk, L. Aloui, N. Prud'homme, B. Sarapata, F. Senocq, D. Samélor, C. Vahlas, ECS Trans. 25 (2009) 581–586.

[16] C. Vahlas, P. Ortiz, D. Oquab, I.W. Hall, J. Electrochem. Soc. 148 (2001) 583–589.

[17] N. Trigoulet, T. Hashimoto, S. Molchan, P. Skeldon, G.E. Thompson, A. Tempez, B. Chapon, Surf. Interface Anal. 42 (2010) 328–333.

[18] R. Payling, M. Aeberhard, D. Delfosse, J. Anal. At. Spectrom. 16 (2001) 50–55.

[19] A. Benali, C. Lacaze-Dufaure, J. Morillo, Surf. Sci. 605 (2011) 341–350.

[20] J.L. Murray, Int. Metals Rev. 30 (1985) 211.

[21] D. Mangelinck, K. Hoummada, I. Blum, Appl. Phys. Lett. 95 (2009) 181902.